Lateral $Si_{0.15}Ge_{0.85}/Ge/Si_{0.15}Ge_{0.85}$ Double-Heterojunction Laser With SiN Stressor

Xinyang Sun, Bin Shu, and Huiyong Hu

***Abstract*—Integrated circuit technology has undergone significant advancements and progress over the past few decades. However, as the demand to further shrink circuit sizes increases, traditional IC interconnections face challenges such as RC delay, energy loss, and interconnect interference, which become increasingly prominent. Optical interconnection emerges as a promising solution to mitigate these issues by enabling reductions in circuit size, power consumption, and signal delay. In this article, we propose a novel lateral $Si_{0.15}Ge_{0.85}/Ge/Si_{0.15}Ge_{0.85}$ p-i-n double-heterojunction laser array, leveraging SiN stress as a key component. Our study focuses on the EL emission properties of individual lasers within the array, the distribution of SiN stress within the device, and the impact of stress on the laser properties. Additionally, we design a $Si_{0.15}Ge_{0.85}/SiO_2$ distributed Bragg reflector (DBR) tailored for the laser array. Simulation results demonstrate a peak luminescence wavelength of 1849 nm and a threshold current density of 190 kA/cm^2 at 300 K.**

***Index Terms*—Photoelectric integration, double-heterojunction laser, SiN stressor, Germanium, DBR.**

I. Introduction

SILICON-BASED photoelectric integration technology is an emerging research field that has gained traction in recent years. The primary objective is to achieve the integration of various electronic devices, such as lasers, optical modulators, optical waveguides, optical detectors, and MOSFETs, onto a single chip. Currently, optoelectronic devices based on Group III-V materials are relatively mature. While Group III-V optoelectronic devices offer superior photoelectric properties due to their direct bandgap characteristics, their compatibility with existing Si-based CMOS technology is challenging due to significant lattice mismatch and large thermal expansion coefficient disparities between Group III-V and Si materials. These issues have presented substantial obstacles to the further advancement of photoelectric integration technology.

Although Germanium (Ge) is an indirect bandgap semiconductor material, it exhibits a relatively small energy difference of only 136 meV between the Γ energy valley at the direct bandgap and the L energy valley at the indirect bandgap, as illustrated in Fig. 1(a). The application of strain to Germanium can induce structural changes, leading to modifications in its energy band structure and subsequent effects on its luminescence properties. Specifically, when tensile strain is applied to Germanium, the lattice undergoes changes that result in a narrowing of the bandgap width. Notably, the Γ energy valley experiences a greater narrowing rate compared to the L energy valley [3]. Consequently, when approximately 1.8% biaxial strain is applied, both the Γ energy valley and L energy valley of Germanium become nearly flat. This transformation allows Germanium to transition into a direct bandgap semiconductor, enabling direct bandgap luminescence and significantly improving luminous efficiency [1], [2], as depicted in Fig. 1.

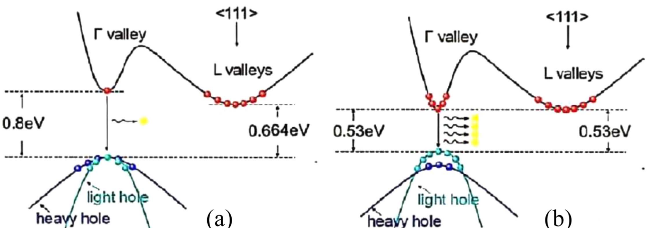

Fig. 1. Band structure of Ge at 300 K (a) unstrained (b) 1.8% tensile strain.

The band structure diagram of the double-heterojunction is shown in Fig. 2(a). In this structure, the band gap width of the material located in the intrinsic region i is narrower compared to the band gap widths of the p and n regions on both sides. As a result, electrons and holes entering the potential well of region i need to overcome a barrier to escape. This characteristic enables the double heterojunction to confine carriers effectively. Fig. 2(b) illustrates the refractive index distribution within the double heterojunction. The refractive index of photons in the n and p regions is lower than that in the i region. Consequently, photons generated through carrier recombination remain confined to the region i. The combined effects of carrier and photon confinement in the double heterojunction facilitate stimulated radiation within region i. As a large number of photons are produced through the recombination of electrons and holes, the photons remain restricted to participating in the process of stimulated radiation within region i. This confinement leads to enhanced stimulated radiation and efficient luminescence. In this study, a double heterojunction structure comprising Ge and

Manuscript received 12 June 2023; revised 18 July 2023; accepted 22 July 2023. Date of publication 25 July 2023; date of current version 8 August 2023. This work was supported by the Ministry of Science and Technology under Project B020250013. *(Corresponding author: Bin Shu.)*

The authors are with the National Key Laboratory of Wide Band Gap Semiconductor, School of microelectronics, Xidian University, Xi'an 710071, China (e-mail: binshu@xidian.edu.cn).

Digital Object Identifier 10.1109/JPHOT.2023.3298682

This work is licensed under a Creative Commons Attribution 4.0 License. For more information, see https://creativecommons.org/licenses/by/4.0/

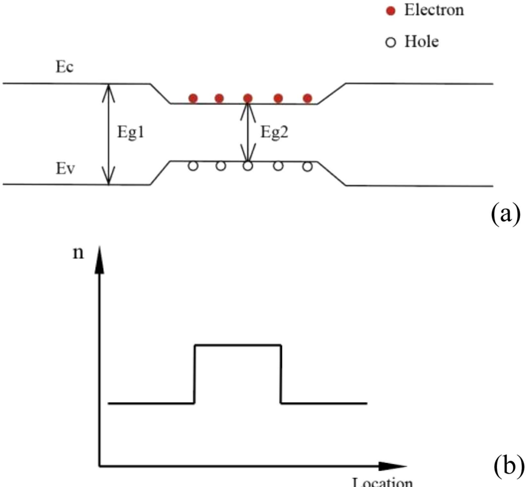

Fig. 2. (a) Schematic diagram of the double heterojunction band structure (b) diagram of the refractive index distribution of the double heterojunction.

the alloy material $Si_{0.15}Ge_{0.85}$ is employed. The Ge-like crystal structure of $Si_{0.15}Ge_{0.85}$, along with the smaller lattice mismatch between $Si_{0.15}Ge_{0.85}$ and Ge compared to Si and Ge, allows for the preparation of high-quality Ge on $Si_{0.15}Ge_{0.85}$ with minimal defects.

II. Device Structure

The 3D schematic diagram and profile structure diagram of the device are presented in Figs. 3 and 4, respectively. The device comprises an SOI substrate, a $Si_{0.5}Ge_{0.5}$ buffer layer, a $Si_{0.15}Ge_{0.85}$ layer, a p-i-n structure, and a DBR resonator. The SOI substrate is employed to minimize device leakage and power consumption. The $Si_{0.5}Ge_{0.5}$ buffer layer serves as an intermediate layer between the Si and Ge materials, reducing lattice mismatch between the layers. The $Si_{0.15}Ge_{0.85}$ layer functions as the P and N regions of the laser. By using the $Si_{0.15}Ge_{0.85}$ alloy as a template, high-quality Ge can be grown, resulting in reduced material defects and improved Ge layer quality. The p-i-n structure of the laser adopts a lateral configuration where the p region, n region, and i region are in the same plane. Ge is etched into a grid structure perpendicular to the substrate, forming the active region between N-type doped $Si_{0.15}Ge_{0.85}$ and P-type $Si_{0.15}Ge_{0.85}$ layers. To introduce biaxial tensile strain into the Ge material, a high-stress Si_3N_4 layer is filled into the groove between two Ge layers.

The distributed Bragg reflector (DBR) is a periodic structure which consists of alternating layers of two materials with different refractive indexes. The optical thickness of each layer is precisely designed to be one-fourth of the Bragg wavelength. When light traverses the DBR, it undergoes resonance within multiple sub-resonators, leading to enhanced laser light intensity. In comparison to Fabry-Perot (FP) lasers, distributed feedback (DFB) lasers employing DBR as the resonator offer several advantages, including single-mode output, excellent monochromatic behavior, and high emission power. Therefore, in this article, a lateral DBR reflector is introduced to enhance the performance of the designed laser. The fabrication process

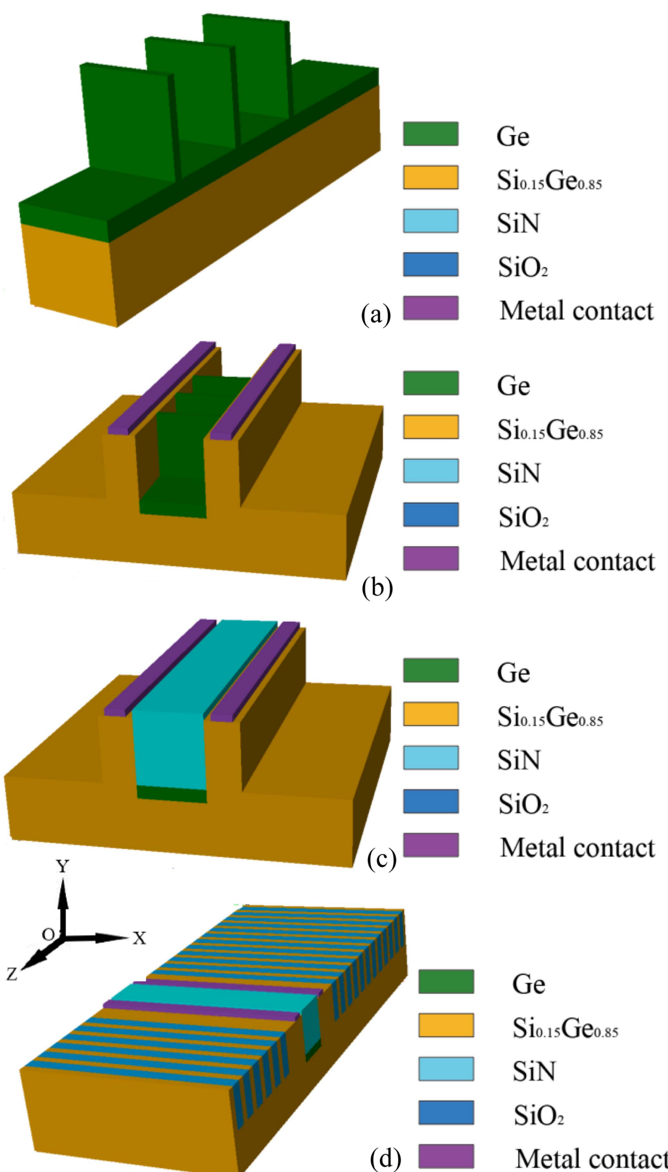

Fig. 3. 3D diagram of lateral $Si_{0.15}Ge_{0.85}$/Ge/$Si_{0.15}Ge_{0.85}$ double-heterojunction laser (a) the active region without SiN (b) the p-i-n structure without SiN (c) the p-i-n structure with Si_3N_4 (d) the overall structure.

of the lateral DBR involves etching grooves on the $Si_{0.15}Ge_{0.85}$ layer and subsequently filling them with SiO_2. This process is compatible with the CMOS process. Through calculations, the optimal dimensions for the DBR structure are determined. Specifically, the width of the etched groove, which corresponds to the thickness of the SiO_2 layer, is found to be 308 nm, while the spacing between each groove, representing the thickness of the $Si_{0.15}Ge_{0.85}$ layer, is determined to be 132 nm. The structure diagram of the DBR is illustrated in Fig. 5.

The laser design proposed in this article offers several notable advantages: 1) The adoption of a lateral laser structure enables multiple laser groups to share the same set of P and N regions. This design approach effectively minimizes the required chip area, leading to space savings and improved integration efficiency. 2) By etching the Ge layer into a thin longitudinal

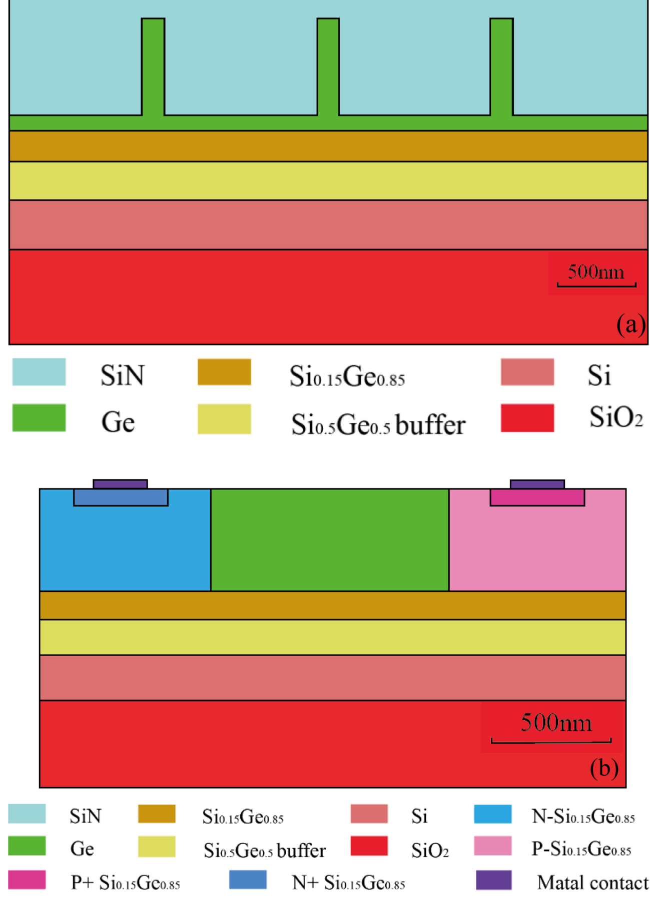

Fig. 4. (a) Profile in XOY of the lateral $Si_{0.15}Ge_{0.85}$/Ge/ $Si_{0.15}Ge_{0.85}$ double-heterojunction laser (b) profile in YOZ of the lateral $Si_{0.15}Ge_{0.85}$/Ge/$Si_{0.15}Ge_{0.85}$ double-heterojunction laser.

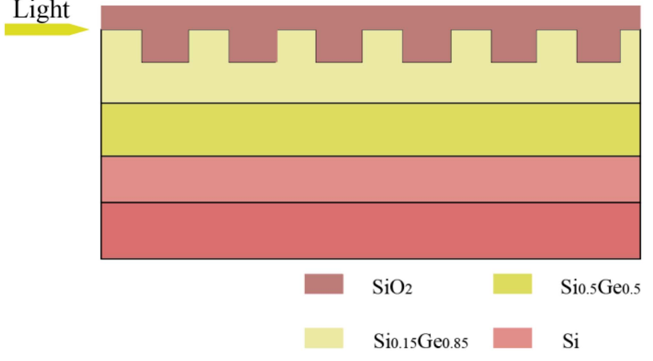

Fig. 5. Profile of the DBR.

structure, the high-stress Si_3N_4 layer can introduce uniform and significant tensile stress into the Ge material. This controlled strain enhances the performance of the laser and contributes to improved optical properties. 3) The incorporation of a distributed Bragg reflector (DBR) into the laser design brings about several benefits. The DBR structure enhances the monochromatic behavior of the lasers, resulting in a more precise and focused emission wavelength. Additionally, the DBR contributes to improved emission power, amplifying the overall performance of the lasers. 4) The laser fabrication process described in this article is compatible with CMOS technology. This compatibility ensures a streamlined manufacturing process by leveraging existing CMOS infrastructure, reducing process complexity, and lowering the overall cost of laser production. These advantages collectively make the proposed laser design highly promising for practical applications, as it addresses key challenges such as chip area utilization, strain engineering, optical performance, and process compatibility, paving the way for cost-effective and efficient laser preparation.

III. Results and Discussion

Through simulation experiments, the relationship between the thickness of the Ge layer and the distribution of tensile stress is obtained, as shown in Fig. 6. The figures labeled (a) to (f) in Fig. 6 display the distribution of tensile stress exerted by the SiN stress layer on the Ge layer for different Ge layer thicknesses, specifically 100 nm, 200 nm, 300 nm, 400 nm, 500 nm, and 600 nm. It is evident from the results that when the thickness of the Ge layer exceeds 500 nm, a significant non-uniform stress distribution occurs. On the other hand, when the thickness of the Ge layer is less than 300 nm, the SiN stressor induces a substantial and uniform stress in the Ge layer. Notably, when the Ge layer is as thin as 100 nm, the SiN stress layer introduces approximately 0.8% biaxial tensile strain into the Ge layer, and this strain is uniformly distributed throughout the Ge layer. These findings demonstrate the crucial role of the SiN stressor in introducing controlled tensile strain into the Ge layer. Moreover, they provide insights into the optimal thickness of the Ge layer for achieving a uniform stress distribution, with a notable strain of 0.8% being achieved when the Ge layer thickness is 100 nm.

The simulation results evaluating the laser properties under different Ge layer thicknesses are presented in Fig. 7. As the Ge layer thickness increases, the stress within the Ge material gradually decreases, while the threshold current of the laser increases. For instance, when the Ge layer thickness is 100 nm, the threshold current density of the laser is approximately 190 kA/cm^2. However, when the Ge layer thickness is extended to 500 nm, the threshold current density exceeds 600 kA/cm^2.Furthermore, a reduction in the Ge layer thickness is accompanied by an increase in the luminous power output and a red shift in the laser emission wavelength. Taking into account both the device properties and the associated technological challenges, the design choice for the laser is to utilize a Ge layer thickness of 100 nm. By selecting a thinner Ge layer, the threshold current density can be minimized while maintaining desirable luminous power and laser emission properties. This decision balances the performance requirements of the laser device with practical considerations related to the fabrication process.

$Si_{0.15}Ge_{0.85}$ alloy forms a double-heterojunction structure with Ge as a barrier. Fig. 8 shows the comparison of the properties between the double-heterojunction devices and the homojunction devices during the period. The barrier formed by the double-heterojunction structure plays an effective role in restrict the carrier. As shown in Fig. 8(a), the laser with

Fig. 6. The stress distribution with Ge thickness of (a) 100 nm (b) 200 nm (c) 300 nm (d) 400 nm (e) 500 nm (f) 600 nm.

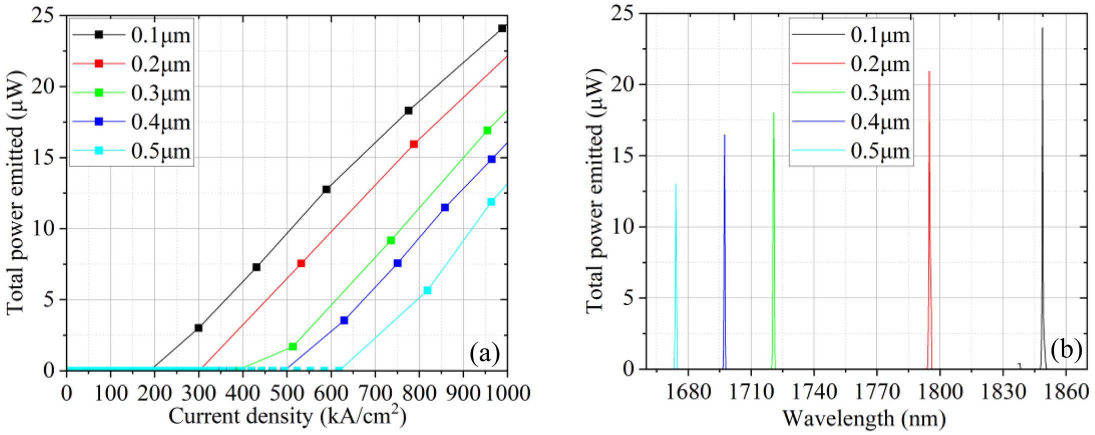

Fig. 7. (a) P-J property under different Ge layer thickness (b) emission spectra under different Ge layer thickness.

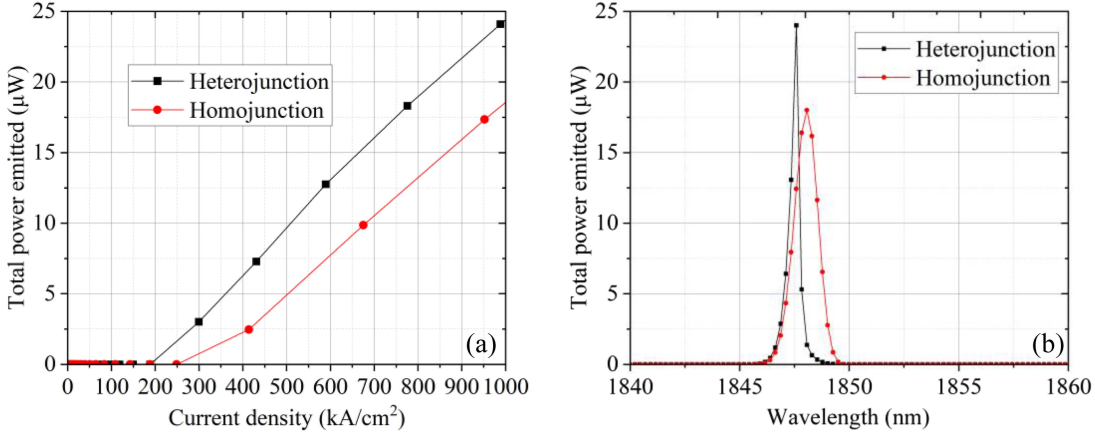

Fig. 8. Property of lasers with double-heterojunction and homojunction structure (a) P-J property (b) emission spectra.

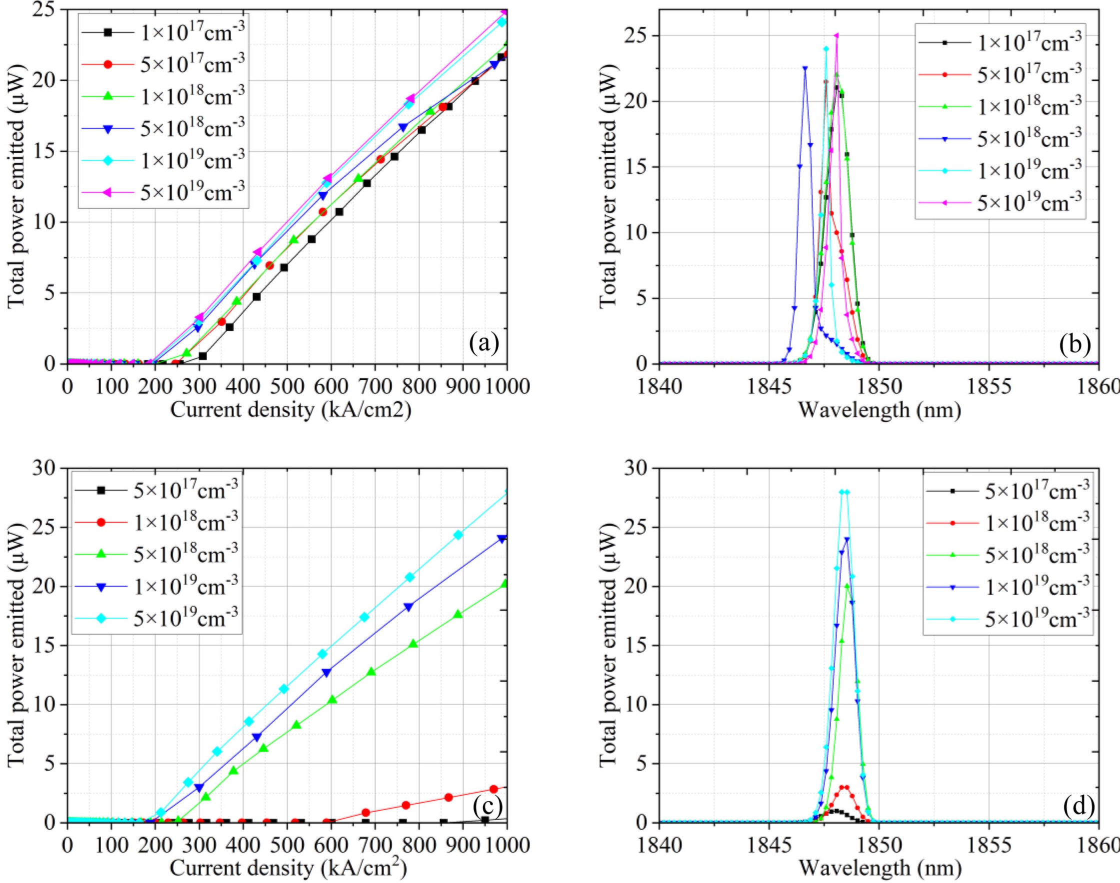

Fig. 9. (a) Influence of N-region doping concentration on P-J property (b) influence of N-region doping concentration on emission spectra (c) influence of P-region doping concentration on P-J property (d) influence of P-region doping concentration on emission spectra.

double-heterojunction structure has a smaller threshold current density, because the restriction effect of double-heterojunction makes laser excitation easier. At the same time, the double-heterojunction laser has better light emission property, not only the emission power is greater than that of the homojunction laser, but also because of the light limitation of the heterogeneous materials, the double-heterojunction laser has better monochromatic behavior, and red shift of the laser is smaller.

In the process of device optimization, we conducted a study on the influence of doping concentration in the N and P regions on the device properties. The simulation results are presented in Fig. 9. Fig. 9(a) illustrates the influence of N-region doping concentration on the P-J characteristics of the device, while Fig. 9(b) shows its impact on the light emission properties. Surprisingly, the doping concentration in the N-region does not have a significant effect on either the threshold property

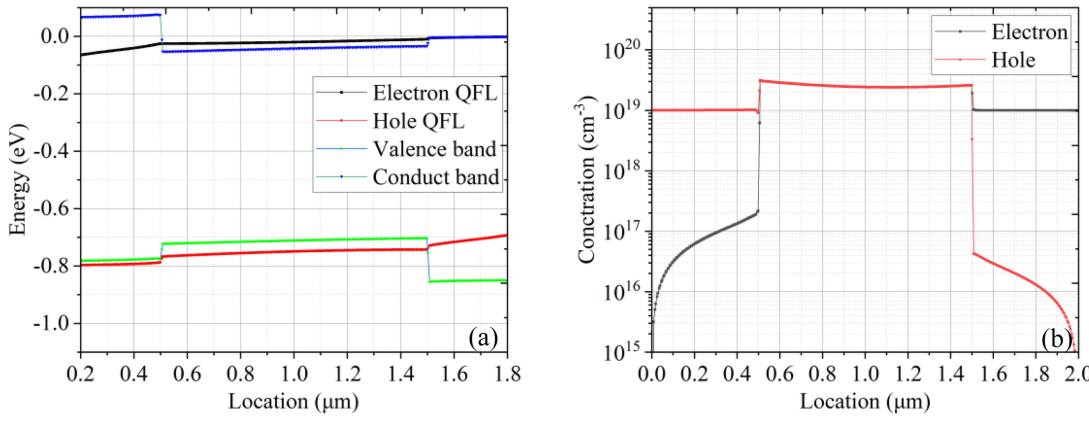

Fig. 10. (a) The energy band and QFL (b) the concentration distribution of electrons an holes.

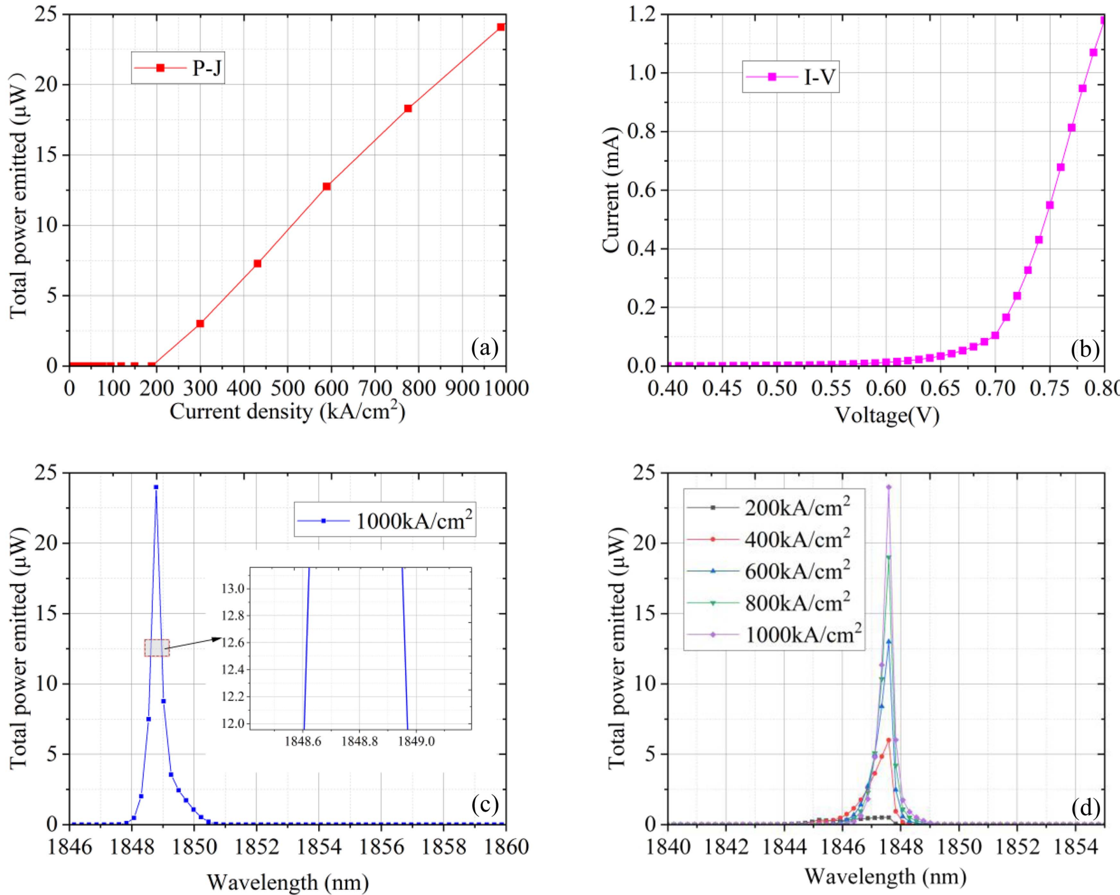

Fig. 11. (a) P-J property (b) I-V property (c) emission spectra under 1000kA/cm^2 (d) emission spectra under different current density.

or the emission property of the device. In contrast, the doping concentration in the P-region plays a crucial role in shaping the device characteristics, as demonstrated in Fig. 9(c) and (d). As the P doping concentration increases, there is a noticeable downward trend in the threshold current of the laser, accompanied by an increase in emission intensity. This behavior can be attributed to the band structure of Ge, where the heterojunction formed by $Si_{0.15}Ge_{0.85}$ and Ge imposes a stronger confinement on holes compared to electrons. Consequently, changes in the hole concentration have a more pronounced impact on the laser properties. Considering the potential effects on the absorption coefficient and the introduction of crystal defects, we have determined the final design parameters for the doping concentrations. The N-region doping concentration is set at 1×10^{19} cm^{-3}, while the P-region doping concentration is 1×10^{19} cm^{-3}. These choices take into account the desired device performance

while minimizing potential detrimental effects associated with excessive doping concentrations and crystal defects. Through extensive simulation of the device structure, we have obtained the band structure diagram of the transverse structure, which is depicted in Fig. 10. The introduction of heterojunction and heavy doping in the N-region has significant effects on the band structure of the active region. As a result, the electron Fermi level appears in the conduction band, while the hole Fermi level appears in the valence band. This configuration enables efficient carrier transport and recombination within the active region, facilitating the generation of photons and achieving desirable laser performance. According to the formula:

$$\mathbf{E_{Fn}-E_{Fq}>E_g}$$

The number of electrons present at the bottom of the high energy conduction band is significantly higher than the number of holes at the top of the low energy valence band. This population inversion is crucial for achieving laser emission in the device. According to the laser emission condition, the rate of excited radiation should exceed the rate of excited absorption. This condition ensures that the device emits coherent light and functions as a laser. The population inversion between the conduction band electrons and valence band holes facilitates the stimulated emission process and allows for the efficient generation of photons.

The laser emission power as a function of current density is depicted in Fig. 11(a). It can be observed that when the current density surpasses 190 kA/cm^2, there is a noticeable surge in the optical emission power. This indicates the onset of laser operation in the device. Furthermore, the emission spectrum of the laser is illustrated in Fig. 11(c). Notably, there is a prominent laser emission peak at the wavelength of 1848.8 nm. Additionally, the half-peak width of the laser emission is confined to approximately 0.4 nm, demonstrating excellent monochromatic behavior.

IV. Conclusion

A lateral $Si_{0.15}Ge_{0.8}$/Ge/$Si_{0.15}Ge_{0.85}$ p-i-n double-heterojunction laser is proposed in this article. By utilizing a palisade structure in the Ge layer with a high-stress Si_3N_4 film, biaxial strain of 0.8% is introduced, which is significantly higher than the strain introduced by directly coating the laser on the surface of Si_3N_4. This approach enables the achievement of an EL emission peak at approximately 1849nm, effectively enhancing the photoelectric conversion efficiency of Ge and reducing the threshold current density of the laser. Moreover, the influence of the $Si_{0.15}Ge_{0.85}$/Ge/ $Si_{0.15}Ge_{0.85}$ double heterojunction structure on the laser is investigated. The presence of $Si_{0.15}Ge_{0.85}$ not only reduces defects and improves the quality of the Ge layer but also effectively lowers the threshold current density of the laser. This results in improved monochromatic behavior and increased luminous power of the laser output. The proposed $Si_{0.15}Ge_{0.85}$/Ge/$Si_{0.15}Ge_{0.85}$ p-i-n double heterojunction laser demonstrates a photoelectric conversion efficiency of 3.95%, which is significantly higher than the typical Ge lasers with an efficiency of less than 1%. Additionally, the threshold current is reduced compared to general Ge lasers. This work provides a feasible solution for realizing Si-based light sources and is compatible with CMOS technology, thereby reducing the production cost of silicon-based photonic integrated chips.

V. Process Flow

1) A $Si_{0.5}Ge_{0.5}$ buffer layer was grown on an SOI substrate using the PECVD process to facilitate a smooth transition between Si and Ge, reducing lattice defects during material growth. 2) The $Si_{0.15}Ge_{0.85}$ layer was deposited onto the $Si_{0.5}Ge_{0.5}$ buffer layer using super vacuum chemical vapor deposition at 350 °C. 3) N and P regions were formed in the $Si_{0.15}Ge_{0.85}$ layer. Ion implantation was employed to create a P-type doping zone with a concentration of 1×10^{19}cm^{-3} and an N-type doping zone with a concentration of 1×10^{19}cm^{-3}. 4) Reactive ion etching technology was utilized to create a 1 μm wide and 1 μm deep groove in the contact region between the P and N zones of the $Si_{0.15}Ge_{0.85}$ layer. 5) The Ge layer was epitaxially grown on the surface of the $Si_{0.15}Ge_{0.85}$ layer and the grooves using molecular beam epitaxy at a growth temperature of 90 °C. This technique enables low-temperature growth of high-quality Ge material. 6) Reactive ion etching was employed to remove the excess Ge material outside the groove. Additionally, grooves with a width of 500 nm and an interval of 100 nm were etched into the Ge layer to form a grid Ge structure. 7) A SiN stress layer was deposited onto the Ge surface using PECVD at 400 °C. The grooves were filled, and the Si_3N_4 layer extending beyond the Ge layer was subsequently etched. 8) Ion implantation was used to create heavily doped ohmic contact regions with a doping concentration of 1×10^{20}cm^{-3} on the N and P regions, respectively. 9) Reactive ion etching technology was employed to create grooves perpendicular to the direction of light on the $Si_{0.15}Ge_{0.85}$ layer at the front and rear ends of the active region structure. These grooves had a width of 308 nm and a spacing of 132 nm. 10) PECVD was used to fill the grooves created in step (8) with SiO_2, forming a distributed Bragg reflector. 11) Metal electrodes were deposited on the P and N regions through sputtering etching and deposition to establish the strip metal electrodes.

References

[1] C. G. V. de Walle, “Band lineups and deformation potentials in the model-solid theory,” *Phys. Rev. B*, vol. 39, no. 3, 1989, Art. no. 1871.
[2] X. Sun et al., “Optical bleaching of thin film Ge on Si,” *Electrochem. Soc. Trans.*, vol. 16, no. 10, pp. 881–889, 2008.
[3] J. Jiang et al., “Analysis of threshold current of uniaxially tensile stressed bulk Ge and Ge/SiGe quantum well lasers,” *Opt. Exp.*, vol. 25, no. 22, pp. 26714–26727, 2017.
[4] M. R. Barget et al., “Tensile strain in Ge membranes induced by SiGe nanostressors,” *Appl. Phys. Lett.*, vol. 109, no. 13, 2016, Art. no. 133109.
[5] J. Liu et al., “Ge laser and on-chip electronic-photonic integration,” in *Proc. 17th Opto-Electron. Commun. Conf.*, 2012, pp. 277–278.
[6] K. Tani, K. Oda, M. Deura, and T. Ido, “Enhanced room-temperature electroluminescence from a Germanium waveguide on a silicon-on-insulator diode with a silicon nitride stressor,” *Opt. Exp.*, vol. 29, no. 3, pp. 3584–3595, 2021.
[7] J. L. Jiang et al., “Strain-induced enhancement of electroluminescence from highly strained Germanium light-emitting diodes (article),” *Amer. Chem. Soc. Photon.*, vol. 6, no. 4, pp. 915–923, 2019.

[8] Q. Senbiao et al., "Monolithic integrated emitting-detecting configuration based on strained Ge microbridge," *Nanophotonics*, vol. 10, no. 11, pp. 2847–2857, 2021.
[9] Y. Jung et al., "Biaxially strained Germanium crossbeam with a high-quality optical cavity for on-chip laser applications," *Opt. Exp.*, vol. 29, no. 10, pp. 14174–14181, 2021.
[10] Z. Qi, H. Sun, M. Luo, Y. Jung, and D. Nam, "Strained Germanium nanowire optoelectronic devices for photonic-integrated circuits," *J. Phys.: Condens. Matter*, vol. 30, no. 33, 2018, Art. no. 334004.
[11] J. Ke, L. Chrostowski, and G. Xia, "Stress engineering with silicon nitride stressors for Ge-on-Si lasers," *IEEE Photon. J.*, vol. 9, no. 2, Apr. 2017, Art. no. 1501615.
[12] G. Y. Lin et al., "Strong room temperature electroluminescence from lateral p-SiGe/i-Ge/n-SiGe heterojunction diodes on silicon-on-insulator substrate," *Appl. Phys. Lett.*, vol. 109, no. 14, 2016, Art. no. 141104.
[13] D. S. Sukhdeo, S. Gupta, K. C. Saraswat, B. R. Dutt, and D. Nam, "Ultimate limits of biaxial tensile strain and n-type doping for realizing an efficient low-threshold Ge laser," *Japanese J. Appl. Phys.*, vol. 55, no. 2, 2016, Art. no. 024301.